PHOTONICS Research

Nonlinear optical properties of WSe_2 and $MoSe_2$ films and their applications in passively *Q*-switched erbium doped fiber lasers

Wenjun Liu,[1,2,3] Mengli Liu,[1] Hainian Han,[1] Shaobo Fang,[2] Hao Teng,[2] Ming Lei,[1,4] and Zhiyi Wei[2,*]

[1]State Key Laboratory of Information Photonics and Optical Communications, School of Science, Beijing University of Posts and Telecommunications, Beijing 100876, China
[2]Beijing National Laboratory for Condensed Matter Physics, Institute of Physics, Chinese Academy of Sciences, Beijing 100190, China
[3]e-mail: jungliu@bupt.edu.cn
[4]e-mail: mlei@bupt.edu.cn
*Corresponding author: zywei@iphy.ac.cn

Received 8 May 2018; revised 8 July 2018; accepted 8 July 2018; posted 12 July 2018 (Doc. ID 330890); published 7 August 2018

Transition metal dichalcogenides (TMDs) are successfully applied in fiber lasers for their photoelectric properties. However, in previous work, how to improve the modulation depth of TMD-based saturable absorbers (SAs) has been a challenging issue. In this paper, WSe_2 and $MoSe_2$ SAs are fabricated with the chemical vapor deposition method. Compared with previous experiments, the modulation depths of WSe_2 and $MoSe_2$ SAs with sandwiched structures are effectively increased to 31.25% and 25.69%, respectively. The all-fiber passively *Q*-switched erbium doped fiber lasers based on WSe_2 and $MoSe_2$ SAs are demonstrated. The signal-to-noise ratios of those lasers are measured to be 72 and 57 dB, respectively. Results indicate that the proposed WSe_2 and $MoSe_2$ SAs are efficient photonic devices to realize stable fiber lasers.

OCIS codes: (160.4330) Nonlinear optical materials; (140.3510) Lasers, fiber.

https://doi.org/10.1364/PRJ.6.000C15

1. INTRODUCTION

In recent years, compact and efficient pulsed lasers have been of great usefulness in applications in the fields of harmonic generation, laser ranging, lidar, and laser processing [1–6]. Generally, active and passive *Q*-switching techniques are two effective methods in *Q*-switched fiber lasers. Differently than the passive one, the actively *Q*-switched technique requires the addition of a modulator (acousto-optic modulator or electro-optic modulator) in the laser cavity [7–9]. Thus, passively *Q*-switched fiber lasers are preferred in applications for the characteristics of high anti-interference and easy integration [10–21].

A saturable absorber (SA) is the key component of a passively *Q*-switched fiber laser [22]. Because of relatively mature production techniques, semiconductor saturable absorber mirrors (SESAMs) have almost dominated commercial markets for SA-based pulsed lasers [23]. However, the complex manufacture and limited bandwidth of SESAMs hinder their further development [24,25]. Carbon nanotubes (CNTs), graphene, black phosphorus (BP), antimonene, and bismuthene are attracting much attention due to the merits of the large third nonlinearity, wide absorption wavelength, and ultrafast recovery time [26–29]. Those materials inspired fresh exploration and efforts in 2D materials. Transition metal dichalcogenides (TMDs), as a burgeoning type of 2D material, have aroused wide interest due to the optical property of being thickness dependent [30–32]. There is a transition of TMDs from an indirect bandgap to a direct bandgap when the material changes from the bulk to single layer, which makes it possible to engineer the bandgap of TMDs [33–42]. This novel feature brings about some excellent optical properties, such as high carrier mobility and outstanding nonlinear optical absorption [43,44]. Theoretically, the bandgap and saturable absorption bandwidth are inversely proportional. Compared with WS_2 and MoS_2, WSe_2 and $MoSe_2$ have similar chemical structures while possessing smaller bandgaps. The direct bandgaps of WS_2, MoS_2, WSe_2, and $MoSe_2$ are 2.1, 1.8, 1.65, and 1.57 eV, respectively. We believe that perhaps WSe_2 and $MoSe_2$ have more potential in broadband absorption.

In the process of mode-locking and *Q*-switching, SAs with high nonlinearity, ultrafast recovery time, and large modulation depth will bring better optical performance. Large modulation depth speeds up the process of pulse narrowing. Moreover, it is beneficial to the occurrence of self-starting [45]. As far as the current research situation is concerned, there are few effective measures focused on optimizing the modulation depth of

TMDs. How to improve the modulation depth of SAs is still the challenging issue.

To improve the modulation depth of 2D materials, the surface-to-volume ratio is a significant aspect to break through. It has been reported that high uniformity will lead to high surface-to-volume ratio [46]. Moreover, the nonlinear optical absorption characteristics of 2D materials are related to the thicknesses of the materials. 2D materials with controllable thicknesses exhibit desired nonlinear absorption characteristics. In this paper, few-layer $MoSe_2$ and WSe_2 SAs with large modulation depth are prepared by the chemical vapor deposition (CVD) method. CVD, as a powerful candidate for the fabrication of layered TMDs, is able to produce films with high crystalline and uniform thickness. Furthermore, the film thickness is easy to control because it is proportional to the deposition time. A sample without polyvinyl acetate (PVA) or polymethyl methacrylate (PMMA) is transferred onto the end face of fiber connectors, and then is assembled into SAs. The surface of the SAs is characterized by atomic force microscopy (AFM) and transmission electron microscopy (TEM). We have successfully fabricated layered WSe_2 and $MoSe_2$ SAs with thicknesses of 1.5 and 3 nm, respectively. Because of the high quality and good transfer technology, the modulation depths of WSe_2 and $MoSe_2$ SAs are significantly increased to 31.25% and 25.69%. Stable *Q*-switched fiber lasers based on WSe_2 and $MoSe_2$ SAs have been implemented separately. Results indicate that WSe_2 and $MoSe_2$ SAs with large modulation depth have broad application prospects in fiber lasers.

2. EXPERIMENT

A. Preparation and Characterization of WSe_2 and $MoSe_2$ SAs

The CVD method, which can synthetize films with controllable thickness and high purity and quality, is promising in the preparation of various 2D materials. Before heating, the MoO_3/WO_3 (0.1 g) and Se (0.5 g) powders are placed in the reaction chamber individually. For $MoSe_2$, the temperature in the reaction zone is heated to 800°C at a constant rate of 15°C/min and held for 25 min. For WSe_2, the WO_3 powder is heated to 920°C at a constant rate of 25°C/min and held for 15 min. During heating, gasified MoO_3/WO_3 and Se vapors mix and react with the assistance of Ar/H_2 mixture gas [Ar of 65 sccm (sccm denotes cubic centimeters per minute at standard temperature and pressure), H_2 of 10 sccm for $MoSe_2$; Ar of 100 sccm and H_2 of 10 sccm for WSe_2]. When temperature falls to room temperature, the layered WSe_2 and $MoSe_2$ films are obtained. With the attachment of the PMMA, WSe_2 and $MoSe_2$ films are prone to detach from the substrate and transfer to the end face of fiber connectors. Acetone is finally used to melt and remove the residue of the PMMA.

AFM is commonly used to measure the thickness of films [47]. The different thicknesses of films with different colors are clearly observed in Figs. 1(a) and 1(d). The function curves of height and lateral distance are measured in Figs. 1(b) and 1(e). The thicknesses of WSe_2 and $MoSe_2$ films are about 1.5 and 3 nm, respectively. From previous work [48,49], the film thickness of 1.5 nm corresponds to 2 or 3 layers, and 3 nm corresponds to 4 or 5 layers. TEM is utilized to minutely investigate the surface microstructure and morphologies of films. As presented in Figs. 1(c) and 1(f), at the length of scale bar of 10 nm, WSe_2 and $MoSe_2$ particles are evenly distributed and neatly arranged.

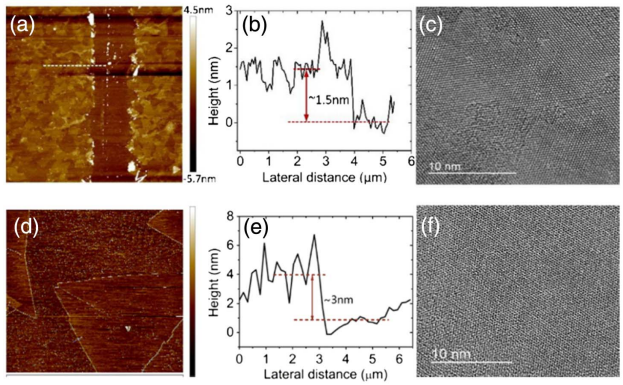

Fig. 1. (a) AFM overview of WSe_2. (b) Function curve of height and lateral distance of the WSe_2 SA. (c) TEM detail image of the WSe_2 SA at scale bar length of 10 nm. (d) AFM image of $MoSe_2$. (e) Function curve of height and lateral distance of the $MoSe_2$ SA. (f) TEM detail image of the $MoSe_2$ SA at high resolution of 10 nm.

From the absorption spectra in Fig. 2, the absorption efficiencies of WSe_2 and $MoSe_2$ SAs are 16.15% and 58.66% at the corresponding bandwidth. To verify whether the light passed the effective area of the films, we observed the distribution of materials with the aid of the microscope. The deep yellow region in Fig. 3(a) is the overlay area of the material, and the light yellow region is the area where the light passes in Fig. 3(b). We can see that the light passes through the center of the films,

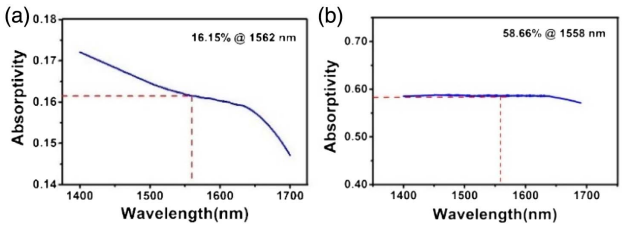

Fig. 2. (a) Absorption spectrum of WSe_2. (b) Absorption spectrum of $MoSe_2$.

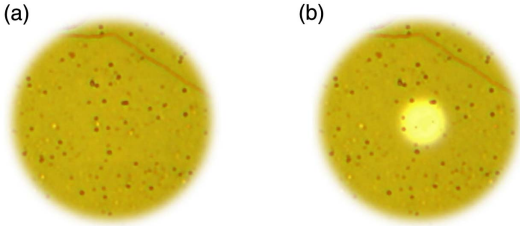

Fig. 3. (a) Effective coverage area of WSe_2 material in the case of no light passing. (b) The light passing through the effective area of material.

which indicates that $MoSe_2$ and WSe_2 films have been completely covered on the effective area of the end face of optical fiber ferrules.

The Raman spectrum of WSe_2 is displayed in Fig. 4(a), in which a pronounced spike at 247 cm^{-1} and a weak peak at 260 cm^{-1} can be observed. The peak at 247 cm^{-1} corresponds to the A_{1g} Raman mode, and the weak peak at 260 cm^{-1} is the second-order peak 2LA(M) because of the appearance of longitudinal acoustic phonons at the M-point in the Brillouin zone. Those results well correspond with previous Raman characteristics of WSe_2 [50]. For $MoSe_2$, the peaks at 241 and 286 cm^{-1} in Fig. 4(b) correspond to the A_{1g} and E^1_{2g} Raman modes, respectively [51]. According to preceding characterization results, the WSe_2 and $MoSe_2$ films fabricated by the CVD method are of high purity and quality. To further explore the saturable absorption properties of WSe_2 and $MoSe_2$ SAs, the balanced twin detector measurement technology is applied. Detailed experimental procedures and schematic diagrams have been presented in previous work [40]. A fiber laser with pulse duration of 600 fs, central wavelength of 1541 nm, and repetition rate of 131 MHz is used as the light source. The data can be well fitted by

$$\alpha(I) = \frac{\alpha_s}{1 + I/I_{\text{sat}}} + \alpha_{ns}, \tag{1}$$

where α_s, α_{ns}, and I_{sat} are the saturable absorption, nonsaturable absorption, and saturation intensity, respectively. The saturation intensity, modulation depth, and corresponding nonsaturable loss of the WSe_2 SA are measured to be 0.734 MW/cm^2, 31.25%, and 54.77%, respectively. For $MoSe_2$, the corresponding saturation intensity, modulation depth, and nonsaturable loss parameters are 9.352 MW/cm^2, 25.69%, and 50.09%, respectively. Large modulation depths are obtained in Figs. 4(c) and 4(d), which show that the WSe_2 and $MoSe_2$ SAs have outstanding saturable absorption properties.

X-ray photoelectron spectroscopy (XPS) is an effective technology to determine the elemental composition of WSe_2 and $MoSe_2$ samples. As shown in Fig. 5(a), the double peaks located at 32.5 and 34.8 eV correspond to the $4f_{7/2}$ and $4f_{5/2}$ binding

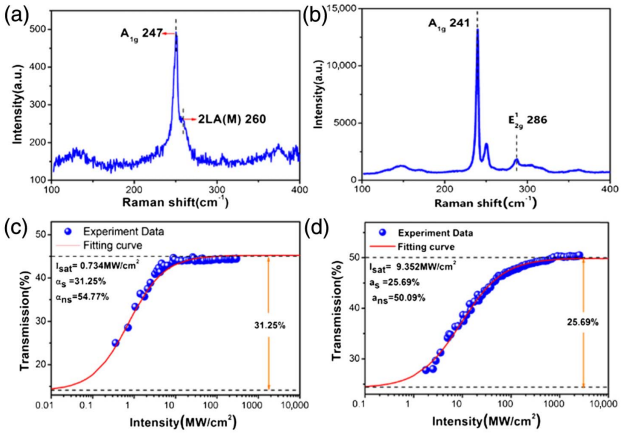

Fig. 4. (a) Raman spectrum of the WSe_2 SA. (b) Raman spectrum of the $MoSe_2$ SA. (c) Non-linear saturable absorption of the WSe_2 SA. (d) Non-linear saturable absorption of the $MoSe_2$ SA.

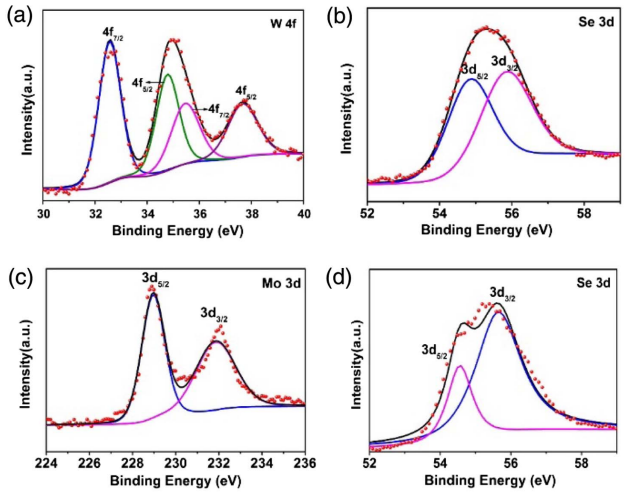

Fig. 5. (a) and (b) are the XPS profiles of WSe_2. (c) and (d) are the XPS profiles of $MoSe_2$.

energies of W, respectively, which indicates the existence of W^{4+}. The peaks at 35.5 and 37.7 eV indicate the presence of W^{6+}, which may come from WO_3. Similarly, the binding energy of Se is shown in Fig. 5(b). Two peaks representing $3d_{5/2}$ and $3d_{3/2}$ of Se are located at 54.9 and 55.9 eV, respectively. The component characterization of W^{4+} and Se indicates the successful synthesis of WSe_2 films on substrates. The presence of W^{6+} indicates there may exist a small amount of WO_3, which is probably due to the oxidation of the edge of the sample. For $MoSe_2$, the double peaks located at 229 and 232 eV correspond to the $3d_{5/2}$ and $3d_{3/2}$ of Mo, respectively, in Fig. 5(c), which confirms the existence of Mo^{4+}. There are no peaks that correspond to Mo^{6+} at 235 eV, which proves that there is no residue of MoO_3 in the sample. The peaks located at 54.5 and 55.6 eV in Fig. 5(d) are generally attributed to Se $3d_{5/2}$ and Se $3d_{3/2}$, respectively. The presence of Mo^{4+} and Se indicates the successful synthesis of $MoSe_2$ films. Moreover, the purity of the sample is high—there is no material residue or oxidation.

B. Experimental Process

The schematic diagram of our experimental installation is shown in Fig. 6. A ring cavity structure is adopted in the passively Q-switched pulse fiber lasers based on WSe_2 and $MoSe_2$ SAs. The ring cavity consists of the polarization independent isolator (PI-ISO), erbium doped fiber (EDF), polarization controller (PC), pump, optical coupler (OC), WSe_2/$MoSe_2$ SA, and wavelength division multiplexer (WDM). The 40 cm long EDF and other optical devices with 1.17 m long single-mode fiber (SMF) are included in the laser cavity. A pump source with center frequency of 976 nm and maximum output power of 680 mW is used in the experiment. The pump light is injected into the cavity through the WDM, 20% of which is extracted by the OC and used for the measurements of experimental results. The PC is able to change the polarization states of the transmitted light, and can be applied to adjust the birefringence in the cavity. The PI-ISO is used to ensure unidirectional transmission of light. The WSe_2 and $MoSe_2$

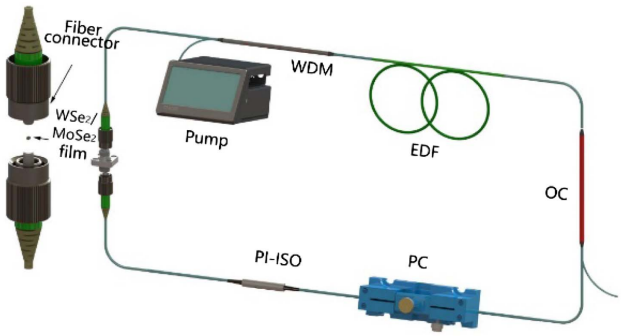

Fig. 6. Schematic diagram of the passively Q-switched pulse fiber laser on the basis of WSe_2 and $MoSe_2$ SAs. Pump is the laser diode with a center wavelength of 976 nm; WDM is the wavelength division multiplexer; WSe_2/$MoSe_2$ SA is the saturable absorber; EDF is the erbium-doped gain fiber; PI-ISO is the polarization independent isolator; PC is the polarization controller; OC is the optical coupler.

films fabricated by the CVD method are transferred onto the end faces of fiber connectors to assemble into WSe_2 and $MoSe_2$ SAs for Q-switched operation. The output pulse trains from the OC are measured by a 500 MHz oscilloscope, an optical spectrum analyzer, and a radio frequency spectrum analyzer.

3. RESULTS AND DISCUSSION

A. WSe_2 SA

By adjusting the PC to optimize the polarization states and properly controlling pump power, stable Q-switched output pulses are observed on the oscilloscope. The starting operation threshold of the Q-switched fiber laser is 110 mW. As we continue to increase pump power, stable Q-switched pulse trains at different power levels are obtained, as presented in Fig. 7(a).

From Fig. 7(b), we obtain a pulse envelope with a symmetrical Gauss shape at the maximum pump power of 680 mW, which indicates that the shortest pulse duration is 1.14 μs. As presented in Fig. 7(c), the optical spectrum of the fiber laser indicates that the central wavelength of the laser is 1562 nm.

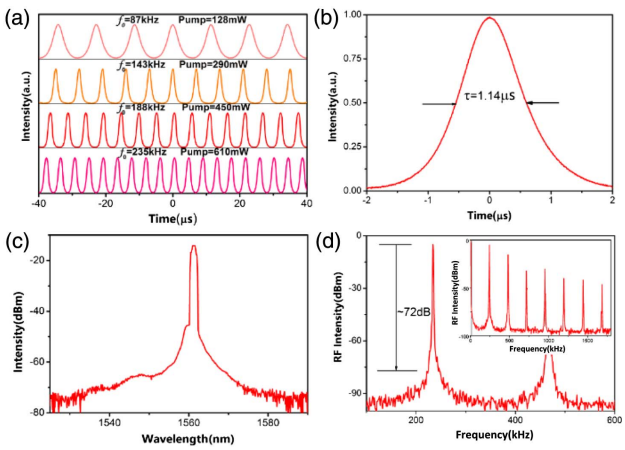

Fig. 7. Experimental results of passively Q-switched pulse fiber laser based on the WSe_2 SA. (a) Pulse trains at different power levels. (b) Single pulse sequence at maximum pump power of 680 mW. (c) Optical spectrum. (d) RF spectrum at 300 Hz RBW.

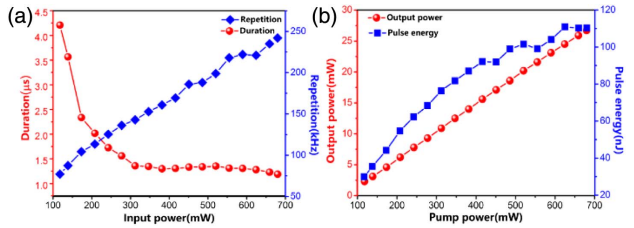

Fig. 8. (a) The trend of repetition and duration as the pump power is boosted. (b) Output power and pulse energy under variable power.

The signal-to-noise ratio (SNR) is measured to be 72 dB at 300 Hz resolution bandwidth (RBW) in Fig. 7(d). The laser is stable over 12 h under laboratory conditions, with no significant degradation in performance.

Through modulating the pump power, the variation tendencies in relevant parameters of the Q-switched fiber laser are summarized in Fig. 8. In Fig. 8(a), the repetition rate of the fiber laser is increasing as the pump power is boosted, but the trend of the pulse duration is opposite to that of the pump power, which is consistent with the inherent characteristics of the Q-switched fiber laser. That is to say, the Q-switched fiber laser is able to achieve stable output pulses at different repetition rates. The adjustable range is 77 to 242 kHz. With the pump power boosting from 110 to 680 mW, the output power of the fiber laser simultaneously increases from 2.3 to 26.7 mW, as shown in Fig. 8(b), and the single pulse energy varies in the range of 30 to 110 nJ.

B. $MoSe_2$ SA

Similar to WSe_2, a stable Q-switched fiber laser is established with the $MoSe_2$ SA. In Fig. 9(a), Q-switched pulse trains at different power levels are shown. The shortest pulse duration is 1.53 μs, as shown in Fig. 9(b). A typical Q-switched output spectrum with central wavelength of 1558 nm is presented in Fig. 9(c). From Fig. 9(d), the SNR of 57 dB indicates the high stability of the Q-switched fiber laser.

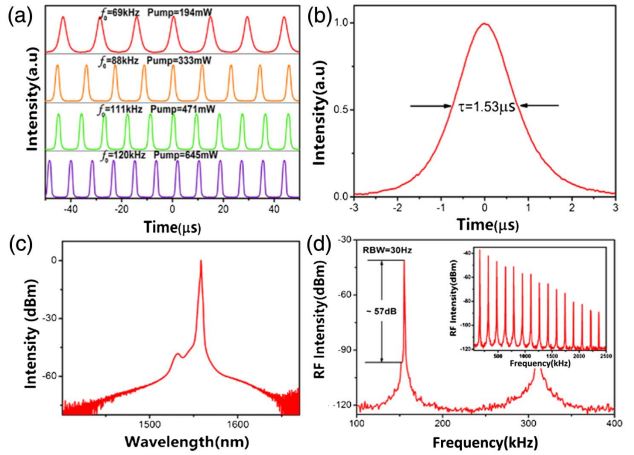

Fig. 9. Experimental results of Q-switched fiber laser based on the $MoSe_2$ SA. (a) Pulse trains at different power levels. (b) Single pulse sequence at maximum pump power of 680 mW. (c) Optical spectrum. (d) RF spectrum.

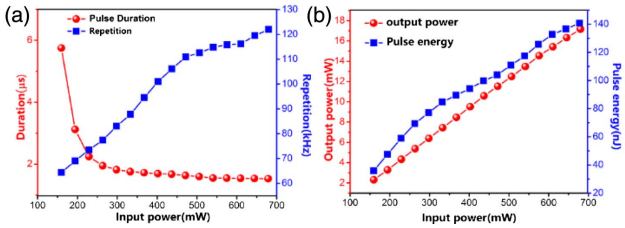

Fig. 10. (a) Trends of repetition and duration as the pump power is boosted. (b) Output power and pulse energy under variable power.

The repetition rates of the fiber laser can be tuned over a range of 64 to 122 kHz when the pump power increases from 160 to 680 mW, as shown in Fig. 10(a). When the pump power is at a lower level, the pulse duration changes more intensely. As the pump power continues to increase, the pulse duration trend is relatively flat, which indicates that the SA tends to be saturated. The single pulse energy and average output power at different power levels are exhibited in Fig. 10(b). When the pump power increases to 680 mW, the maximum output power and single pulse energy are 17.2 mW and 140.6 nJ, respectively.

A comparison of the passively *Q*-switched fiber laser based on WSe_2 and $MoSe_2$ SAs among previous and current works is presented in Tables 1 and 2. It is found that the modulation depths of WSe_2 and $MoSe_2$ SAs in this paper are much larger compared to previous experimental materials. We attribute the success of better performance to the potentially promising CVD approach. The ability to manufacture thin films with high uniformity is a major superiority of the CVD approach. High SNR of 72 dB/57 dB corresponding to our *Q*-switched fiber lasers indicates that the proposed WSe_2 and $MoSe_2$ SAs are efficient photonic devices to realize highly stable fiber lasers. Performance comparisons with MoS_2-based *Q*-switched pulse fiber lasers are also provided in Table 3. We find that the *Q*-switched fiber laser based on the WSe_2 and $MoSe_2$ SAs has a prominent performance in terms of high output power compared with previous *Q*-switched fiber lasers based on MoS_2 SAs. Results indicate that higher output power may be obtained

Table 1. Performance Comparison of the Passively *Q*-Switched Fiber Laser Based on the WSe_2 SA[a]

Materials	Preparation Method	Modulation Depth (%)	Repetition Rate (kHz)	Pulse Duration (μs)	SNR (dB)	*Q*-Switching Threshold (mW)	*P* (mW)	Maximum Pulse Energy (nJ)	Ref.
WSe_2-PVA	LPE	3.5	4.5–49.6	3.1–7.9	46.7	140	1.23	33.2	[52]
WSe_2-PVA	LPE	4.31	92.5–138	0.75–1.48	50	170	3.54	29	[53]
WSe_2-PVA	LPE	3.02	46.3–85.4	4.0–9.2	41.9	280	3.16	484.8	[54]
WSe_2	CVD	31	77–242	1.2–4.3	72	118	26.7	110	This Work

[a]SNR, signal-to-noise ratio; *P*, average output power.

Table 2. Performance Comparison of the Passively *Q*-Switched Fiber Laser Based on the $MoSe_2$ SA

Materials	Preparation Method	Modulation Depth (%)	Repetition Rate (kHz)	Pulse Duration (μs)	SNR (dB)	*Q*-Switching Threshold (mW)	*P* (mW)	Maximum Pulse Energy (nJ)	Ref.
$MoSe_2$-PVA	LPE	6.73	60.724–66.847	4.04–6.506	31.3	570	2.45	369.5	[54]
$MoSe_2$-PVA	ME	4.7	26.5–35.4	4.8–7.9	—	18.9	—	825	[55]
$MoSe_2$-PVA	LPE	1.2	34.5–90	1	35.97	110	2	2.3	[56]
$MoSe_2$-PVA	LPE	0.63	9.9	13.6	—	10	—	—	[57]
$MoSe_2$	CVD	25.69	64–122	1.53–5.75	57	160	17.16	140.7	This Work

Table 3. Performance Comparison with MoS_2-Based *Q*-Switched Fiber Lasers

Materials	Preparation Method	Modulation Depth (%)	Repetition Rate (kHz)	Pulse Duration (μs)	SNR (dB)	*Q*-Switching Threshold (mW)	*P* (mW)	Maximum Pulse Energy (nJ)	Ref.
MoS_2-PVA	LPE	2	8.77–43.47	3.3	50	18.9	5.91	160	[58]
MoS_2-PVA	LPE	2.15	7.758–41.452	9.92	48.5	50	0.77	184.7	[54]
MoS_2-PVA	LPE	1.6	6.5–27.0	5.4	54.6	17.4	1.7	63.2	[17]
MoS_2-PVA	LPE	4	72.74–86.39	3.53	51.6	258	6.47	74.93	[59]
MoS_2	CVD	33.2	10.6–173.1	1.66	42.5	20.4	4.71	27.2	[31]
MoS_2	CVD	28.5%	28.6–114.8	2.18	41.1	42	<1	8.2	[32]
WSe_2	CVD	31%	77–242	1.2	72	118	26.7	110	This Work
$MoSe_2$	CVD	25.69%	64–122	1.53	57	160	17.16	140.7	This Work

if the cavity loss is further reduced, and the pump power increases.

4. CONCLUSIONS

In this paper, layered CVD-grown WSe_2 and $MoSe_2$ films without PVA or PMMA have been proved to have the modulation functions in *Q*-switched fiber lasers. The CVD method has been used to optimize the film uniformity and regulate the film thickness. Therefore, the crystallinity and uniformity as significant influencing factors of the modulation depth have been improved. The modulation depths of WSe_2 and $MoSe_2$ SAs with sandwiched structures have been effectively upgraded to 31.25% and 25.69%, respectively. The fabricated WSe_2 and $MoSe_2$ SAs have achieved stable pulse generation in passively *Q*-switched fiber lasers with SNRs of 72 and 57 dB, respectively, which are the highest among the same type fiber lasers. The superiorities in nonlinearity and uniformity of the fabricated SAs make WSe_2 and $MoSe_2$ promising materials for preparing photonic devices.

Funding. National Natural Science Foundation of China (NSFC) (11674036); Beijing Youth Top-Notch Talent Support Program (2017000026833ZK08); Beijing University of Posts and Telecommunications (BUPT) (IPOC2016ZT04, IPOC2017ZZ05).

REFERENCES

1. R. Paschotta, R. Häring, E. Gini, H. Melchior, U. Keller, H. L. Offerhaus, and D. J. Richardson, "Passively *Q*-switched 0.1 mJ fiber laser system at 1.53 μm," Opt. Lett. **24**, 388–390 (1999).
2. H. Jeong, S. Y. Choi, M. H. Kim, F. Rotermund, Y. H. Cha, D. Y. Jeong, S. B. Lee, K. Lee, and D. Yeom, "All-fiber Tm-doped soliton laser oscillator with 6 nJ pulse energy based on evanescent field interaction with monoloayer graphene saturable absorber," Opt. Express **24**, 14152–14158 (2016).
3. U. Keller, K. J. Weingarten, F. X. Kartner, D. Kopf, B. Braun, I. D. Jung, R. Fluck, C. Honninger, N. Matuschek, and J. Aus der Au, "Semiconductor saturable absorber mirrors (SESAM's) for femtosecond to nanosecond pulse generation in solid-state lasers," IEEE J. Sel. Top. Quantum Electron. **2**, 435–453 (1996).
4. X. Liu, Y. Cui, D. Han, X. Yao, and Z. Sun, "Distributed ultrafast fibre laser," Sci. Rep. **5**, 9101 (2015).
5. H. Chen, Y. S. Chen, J. D. Yin, X. J. Zhang, T. Guo, and P. G. Yan, "High-damage-resistant tungsten disulfide saturable absorber mirror for passively *Q*-switched fiber laser," Opt. Express **24**, 16287–16296 (2016).
6. X. T. Xu, J. P. Zhai, J. S. Wang, Y. P. Chen, and Y. Q. Yu, "Passively *Q*-switching induced by the smallest single-walled carbon nanotubes," Appl. Phys. Lett. **104**, 171107 (2014).
7. S. X. Liu, Z. J. Li, Y. Q. Ge, H. D. Wang, R. Yue, X. T. Jiang, J. Q. Li, Q. Wen, and H. Zhang, "Graphene/phosphorene nano-heterojunction: facile synthesis, nonlinear optics, and ultrafast photonics applications with enhanced performance," Photon. Res. **5**, 662–668 (2017).
8. D. Li, H. Xue, M. Qi, Y. D. Wang, S. Aksimsek, N. Chekurov, W. Kim, C. F. Li, J. Riikonen, F. W. Ye, Q. Dai, Z. Y. Ren, J. T. Bai, T. Hasan, H. Lipsanen, and Z. P. Sun, "Graphene actively *Q*-switched lasers," 2D Mater. **4**, 025095 (2017).
9. Y. Chen, G. B. Jiang, S. Q. Chen, Z. N. Guo, X. F. Yu, C. J. Zhao, H. Zhang, Q. L. Bao, S. C. Wen, D. Y. Tang, and D. Y. Fan, "Mechanically exfoliated black phosphorus as a new saturable absorber for both *Q*-switching and mode-locking laser operation," Opt. Express **23**, 12823–12833 (2015).
10. S. Yamashita, Y. Inoue, S. Maruyama, Y. Murakami, H. Yaguchi, M. Jablonski, and S. Y. Set, "Saturable absorbers incorporating carbon nanotubes directly synthesized onto substrates and fibers and their application to mode-locked fiber lasers," Opt. Lett. **29**, 1581–1583 (2004).
11. M. Zhang, R. C. T. Howe, R. I. Woodward, E. J. R. Kelleher, F. Torrisi, G. H. Hu, S. V. Popov, J. R. Taylor, and T. Hasan, "Solution processed MoS_2-PVA composite for subbandgap mode-locking of a wideband tunable ultrafast Er:fiber laser," Nano Res. **8**, 1522–1534 (2015).
12. M. Zhang, G. H. Hu, G. Q. Hu, R. C. T. Howe, L. Chen, Z. Zheng, and T. Hasan, "Yb- and Er-doped fiber laser *Q*-switched with an optically uniform, broadband WS_2 saturable absorber," Sci. Rep. **5**, 17482 (2015).
13. K. Wu, B. H. Chen, X. Y. Zhang, S. F. Zhang, C. S. Guo, C. Li, P. S. Xiao, J. Wang, L. J. Zhou, W. W. Zou, and J. P. Chen, "High-performance mode-locked and *Q*-switched fiber lasers based on novel 2D materials of topological insulators, transition metal dichalcogenides and black phosphorus: review and perspective," Opt. Commun. **406**, 214–229 (2018).
14. A. Martinez and Z. Sun, "Nanotube and graphene saturable absorbers for fibre lasers," Nat. Photonics **7**, 842–845 (2013).
15. Z. Luo, M. Zhou, J. Weng, G. Huang, H. Xu, C. Ye, and Z. Cai, "Graphene-based passively *Q*-switched dual-wavelength erbium-doped fiber laser," Opt. Lett. **35**, 3709–3711 (2010).
16. Q. Bao, H. Zhang, B. Wang, Z. Ni, C. H. Y. X. Lim, Y. Wang, D. Tang, and K. P. Loh, "Broadband graphene polarizer," Nat. Photonics **5**, 411–415 (2011).
17. Z. Luo, Y. Huang, M. Zhong, Y. Li, J. Wu, B. Xu, H. Xu, Z. Cai, J. Peng, and J. Weng, "1-, 1.5-, and 2-μm fiber lasers *Q*-switched by a broadband few-layer MoS_2 saturable absorber," J. Lightwave Technol. **32**, 4679–4686 (2014).
18. R. I. Woodward, E. J. R. Kelleher, R. C. T. Howe, G. Hu, F. Torrisi, T. Hasan, S. V. Popov, and J. R. Taylor, "Tunable *Q*-switched fiber laser based on saturable edge-state absorption in few-layer molybdenum disulfide (MoS_2)," Opt. Express **22**, 31113–31122 (2014).
19. C. Zhao, H. Zhang, X. Qi, Y. Chen, and Z. Wang, "Ultra-short pulse generation by a topological insulator based saturable absorber," Appl. Phys. Lett. **101**, 211106 (2012).
20. H. Zhang, C. Liu, X. Qi, X. Dai, Z. Fang, and S. Zhang, "Topological insulators in Bi_2Se_3, Bi_2Te_3 and Sb_2Te_3 with a single Dirac cone on the surface," Nat. Phys. **5**, 438–442 (2009).
21. P. Tang, X. Zhang, C. Zhao, Y. Wang, H. Zhang, D. Shen, S. Wen, D. Tang, and D. Fan, "Topological insulator: Bi_2Te_3 saturable absorber for the passive *Q*-switching operation of an in-band pumped 1645-nm Er:YAG ceramic laser," IEEE Photon. J. **5**, 1500707 (2013).
22. R. I. Woodward and E. J. R. Kelleher, "2D saturable absorbers for fibre lasers," Appl. Sci. **5**, 1440–1456 (2015).
23. B. Braun, F. Kärtner, G. Zhang, M. Moser, and U. Keller, "56-ps passively *Q*-switched diode-pumped microchip laser," Opt. Lett. **22**, 381–383 (1997).
24. Z. P. Sun, A. Martinez, and F. Wang, "Optical modulators with 2D layered materials," Nat. Photonics **10**, 227–238 (2016).
25. K. Park, J. Lee, Y. T. Lee, W. K. Choi, J. H. Lee, and Y. W. Song, "Black phosphorus saturable absorber for ultrafast mode-locked pulse laser via evanescent field interaction," Ann. Phys. **527**, 770–776 (2015).
26. H. Lee, W. S. Kwon, J. H. Kim, D. Kang, and S. Kim, "Polarization insensitive graphene saturable absorbers using etched fiber for highly stable ultrafast fiber lasers," Opt. Express **23**, 22116–22122 (2015).
27. Z. Guo, S. Chen, Z. Wang, Z. Yang, F. Liu, Y. Xu, J. Wang, Y. Yi, H. Zhang, L. Liao, P. K. Chu, and X. Yu, "Metal-ion-modified black phosphorus with enhanced stability and transistor performance," Adv. Mater. **29**, 1703811 (2017).
28. Y. Song, Z. Liang, X. Jiang, Y. Chen, Z. Li, L. Lu, Y. Ge, K. Wang, J. L. Zheng, S. B. Lu, J. H. Ji, and H. Zhang, "Few-layer antimonene decorated microfiber: ultra-short pulse generation and all-optical thresholding with enhanced long term stability," 2D Mater. **4**, 045010 (2017).
29. L. Lu, Z. Liang, L. Wu, Y. Chen, Y. Song, S. C. Dhanabalan, J. S. Ponraj, B. Dong, Y. Xiang, F. Xing, D. Fan, and H. Zhang, "Few-layer bismuthene: sonochemical exfoliation, nonlinear optics and applications for ultrafast photonics with enhanced stability," Laser Photon. Rev. **12**, 1700221 (2017).

30. H. D. Xia, H. P. Li, C. Y. Lan, C. Li, X. X. Zhang, S. J. Zhang, and Y. Liu, "Ultrafast erbium-doped fiber laser mode-locked by a CVD-grown molybdenum disulfide (MoS_2) saturable absorber," Opt. Express **22**, 17341–17348 (2014).
31. H. P. Li, H. D. Xia, C. Y. Lan, C. Li, X. X. Zhang, J. F. Li, and Y. Liu, "Passively *Q*-switched erbium-doped fiber laser based on few-layer MoS_2 saturable absorber," IEEE Photon. Technol. Lett. **27**, 69–72 (2015).
32. H. Xia, H. Li, C. Lan, C. Li, J. Du, S. Zhang, and Y. Liu, "Few-layer MoS_2 grown by chemical vapor deposition as a passive *Q*-switcher for tunable erbium-doped fiber lasers," Photon. Res. **3**, A92–A96 (2015).
33. S. F. Zhang, N. N. Dong, N. McEvoy, M. O'Brien, S. Winters, N. C. Berner, C. Yim, X. Y. Zhang, Z. H. Chen, L. Zhang, G. S. Duesberg, and J. Wang, "Direct observation of degenerate two-photon absorption and its saturation in WS_2 and MoS_2 monolayer and few-layer films," ACS Nano **9**, 7142–7150 (2015).
34. X. Y. Zhang, S. F. Zhang, C. X. Chang, Y. Y. Feng, Y. X. Li, N. N. Dong, K. P. Wang, L. Zhang, W. J. Blau, and J. Wang, "Facile fabrication of wafer-scale MoS_2 neat films with enhanced third-order nonlinear optical performance," Nanoscale **7**, 2978–2986 (2015).
35. P. G. Yan, H. Chen, J. Yin, Z. Xu, J. Li, Z. Jiang, W. Zhang, J. Wang, I. L. Li, Z. Sun, and S. Ruan, "Large-area tungsten disulfide for ultrafast photonics," Nanoscale **9**, 1871–1877 (2017).
36. D. Mao, Y. Wang, C. Ma, L. Han, B. Jiang, X. Gan, S. Hua, W. Zhang, T. Mei, and J. Zhao, "WS_2 mode-locked ultrafast fiber laser," Sci. Rep. **5**, 7965 (2015).
37. K. Wu, X. Zhang, J. Wang, X. Li, and J. Chen, "WS_2 as a saturable absorber for ultrafast photonic applications of mode-locked and *Q*-switched lasers," Opt. Express **23**, 11453–11461 (2015).
38. P. G. Yan, A. J. Liu, Y. S. Chen, H. Chen, S. C. Ruan, C. Y. Guo, S. F. Chen, I. L. Li, H. P. Yang, J. G. Hu, and G. Z. Cao, "Microfiber-based WS_2-film saturable absorber for ultra-fast photonics," Opt. Mater. Express **5**, 479–489 (2015).
39. W. Liu, L. Pang, H. Han, K. Bi, M. Lei, and Z. Wei, "Tungsten disulphide for ultrashort pulse generation in all-fiber lasers," Nanoscale **9**, 5806–5811 (2017).
40. W. Liu, L. Pang, H. Han, M. Liu, M. Lei, S. Fang, H. Teng, and Z. Wei, "Tungsten disulfide saturable absorbers for 67 fs mode-locked erbium-doped fiber lasers," Opt. Express **25**, 2950–2959 (2017).
41. D. Mao, B. B. Du, D. X. Yang, S. L. Zhang, Y. D. Wang, W. D. Zhang, X. Y. She, H. C. Cheng, H. B. Zeng, and J. L. Zhao, "Nonlinear saturable absorption of liquid-exfoliated molybdenum/tungsten ditelluride nanosheets," Small **12**, 1489–1497 (2016).
42. J. T. Wang, Z. K. Jiang, H. Chen, J. R. Li, J. D. Yin, J. Z. Wang, T. C. He, P. G. Yan, and S. C. Ruan, "Magnetron sputtering deposited WTe_2 for ultrafast thulium-doped fiber laser," Opt. Lett. **42**, 5010–5013 (2017).
43. K. F. Mak, C. Lee, J. Hone, J. Shan, and T. F. Heinz, "Atomically thin MoS_2: a new direct-gap semiconductor," Phys. Rev. Lett. **105**, 136805 (2010).
44. L. Pang, W. Liu, W. Tian, H. Han, and Z. Wei, "Nanosecond hybrid *Q*-Switched Er-doped fiber laser with WS_2 saturable absorber," IEEE Photon. J. **8**, 1501907 (2016).
45. D. Mao, X. She, B. Du, D. Yang, W. Zhang, K. Song, and J. Zhao, "Erbium-doped fiber laser passively mode locked with few-layer $WSe_2/MoSe_2$ nanosheets," Sci. Rep. **6**, 23583 (2016).
46. R. Wei, H. Zhang, X. Tian, T. Qiao, Z. Hu, Z. Chen, X. He, Y. Yu, and J. Qiu, "MoS_2 nanoflowers as high performance saturable absorbers for an all-fiber passively *Q*-switched erbium-doped fiber laser," Nanoscale **8**, 7704–7710 (2016).
47. C. Prein, N. Warmbold, Z. Farkas, M. Schieker, A. Aszodi, and H. Clausen-Schaumann, "Structural and mechanical properties of the proliferative zone of the developing murine growth plate cartilage assessed by atomic force microscopy," Matrix Biol. **50**, 1–15 (2016).
48. H. Fang, S. Chuang, T. C. Chang, K. Takei, and T. Takahashi, "High-performance single layered WSe_2 p-FETs with chemically doped contacts," Nano Lett. **12**, 3788–3792 (2012).
49. J. Xia, X. Huang, L. Z. Liu, M. Wang, L. Wang, and B. Huang, "CVD synthesis of large-area, highly crystalline $MoSe_2$ atomic layers on diverse substrates and application to photodetectors," Nanoscale **6**, 8949–8955 (2014).
50. M. Yang, X. Cheng, Y. Li, Y. Ren, M. Liu, and Z. Qi, "Anharmonicity of monolayer MoS_2, $MoSe_2$, and WSe_2: a Raman study under high pressure and elevated temperature," Appl. Phys. Lett. **110**, 093108 (2017).
51. S. Tongay, J. Zhou, C. Ataca, K. Lo, T. S. Matthews, and J. Li, "Thermally driven crossover from indirect toward direct bandgap in 2D semiconductors: $MoSe_2$ versus MoS_2," Nano Lett. **12**, 5576–5580 (2012).
52. B. Chen, C. Guo, K. Wu, J. Chen, X. Zhang, and J. Wang, "Tungsten diselenide *Q*-switched erbium-doped fiber laser," Opt. Eng. **55**, 081306 (2016).
53. C. Guo, B. Che, H. Wang, X. Zhang, J. Wang, K. Wu, and J. Chen, "Investigation on the stability of WSe_2-PVA saturable absorber in an all PM *Q*-switched fiber laser," IEEE Photon. J. **8**, 1503612 (2016).
54. B. Chen, X. Zhang, K. Wu, H. Wang, J. Wang, and J. Chen, "*Q*-switched fiber laser based on transition metal dichalcogenides MoS_2, $MoSe_2$, WS_2, and WSe_2," Opt. Express **23**, 26723–26737 (2015).
55. R. I. Woodward, R. C. T. Howe, T. H. Runcorn, G. Hu, F. Torrisi, E. J. R. Kelleher, and T. Hasan, "Wideband saturable absorption in few-layer molybdenum diselenide ($MoSe_2$) for *Q*-switching Yb-, Er- and Tm-doped fiber lasers," Opt. Express **23**, 20051–20061 (2015).
56. H. Ahmad, M. A. Ismail, S. Sathiyan, and S. A. Reduan, "S-band *Q*-switched fiber laser using $MoSe_2$ saturable absorber," Opt. Commun. **382**, 93–98 (2017).
57. Z. Luo, Y. Li, M. Zhong, Y. Huang, and X. Wan, "Nonlinear optical absorption of few-layer molybdenum diselenide ($MoSe_2$) for passively mode-locked soliton fiber laser," Photon. Res. **3**, A79–A86 (2015).
58. J. Ren, S. Wang, Z. Cheng, H. Yu, H. Zhang, Y. Chen, L. Mei, and P. Wang, "Widely-tunable, passively *Q*-switched erbium-doped fiber laser with few-layer MoS_2 saturable absorber," Opt. Express **23**, 5607–5613 (2015).
59. Y. Huang, Z. Luo, Y. Li, M. Zhong, B. Xu, K. Che, H. Xu, Z. Cai, J. Peng, and J. Weng, "Pulsed erbium-doped fiber laser by a few-layer molybdenum disulfide saturable absorber: from *Q*-switching to mode-locking," Opt. Express **22**, 25258–25266 (2014).